

600V Pre-charge control circuit

Hanze Institute of Engineering

Dimitriy Georgiev, Richard Kaiva, Pedro Henrique Wo de Alcantara, Hristiyan Georgiev, Rianne Drijver

Written by Dimitriy Georgiev and Richard Kaiva

January 31, 2021

Abstract—One of the challenges that arise in tractive systems of electric cars is establishing a reliable connection between the accumulator and inverter. The presented pre-charge control circuit is a potential solution that can be used to operate a DC contractor and prevent the flow of high inrush current into the inverter. The circuit has been simulated in LTspice and tested in real life across the temperature range of +10 °C to +65 °C. Pre-charging is stopped once the inverter voltage exceeds 98% of the voltage level of the accumulator and resumed when it is below 95%.

Index Terms—tractive system, pre-charge, inrush current, LTspice

I. INTRODUCTION

Electric vehicles (EVs) have been rising in popularity, in recent years, in accordance with the increased technological development and focus on renewable energy [1]. This creates demand for production of safe and high-performing EVs. In order to produce such vehicles, a number of challenges need to be overcome in the design of the cars. One essential part of EVs is their tractive system, which carries the necessary energy to power the electric motor(s) [2]. This paper explores one of the challenges that arise due to the high voltage levels used in tractive systems of electric cars, namely establishing a reliable connection between an accumulator and an inverter. The capacitive nature of the inverter inputs allows the flow of high inrush current which, if left unlimited, will damage the battery cells, contractors, and inverter itself [3], [4]. For this reason, the research focuses on designing a pre-charge control circuit that will limit the inrush current while the capacitors on the DC side of the inverter charge to at least 95% of the voltage level of the accumulator. The presented circuit is tailored to the needs of the electric racing car of Hanze Racing Division (HARD) - HRD05-2, and adheres to Formula Student Germany (FSG) rules [2]. Ultimately, the research attempts to find an answer to the question - how to safely measure and compare high voltages during pre-charge. Voltage measurement and comparison are requisite for monitoring the performance of the tractive system and establishing control over the pre-charge behaviour. Figure 1 illustrates the desired aspects and functionality of the complete pre-charge circuit.

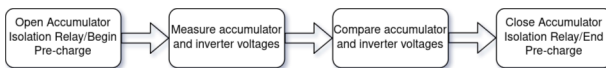


Fig. 1. Generalized block diagram of the desired pre-charge circuit.

A number of possible solutions, inspired from common practices in the automotive industry, were considered in the attempt to implement this functionality. Commercially available multimeters are capable of measuring voltages up to 1000V [5]. One way to achieve such measurements requires stepping down the high voltage level to a lower one through a resistive divider [6]. Stepping down the voltage levels of the accumulator and the inverter also allows for comparison of the two signals with a Comparator integrated circuit (IC). The accuracy of this method is directly affected by the tolerance of the resistors used in the divider to create the step down ratio. Furthermore, common factors to the environment of the racing car, such as temperature and humidity fluctuations, exposure to vibration or shock can trigger failure modes in the circuitry, which will further reduce the reliability of the method. Hence the importance of selecting components with suitable ratings.

II. METHODS

During this project a Design for Six Sigma methodology [7] was applied to create the requested pre-charge circuit. Choosing to follow this approach implied that the project group had to go through several different design stages, before arriving at a product that meets client expectations. The initial phase of the project involved establishing clear customer requirements and technical specifications based on information that has been gathered from documentation and interviews with the client [3]. These requirements and specifications included:

- Pre-charge must be stopped after the inverter voltage has surpassed 95% of the accumulator voltage.
- Intermediate components must galvanically isolate the high voltage system from the low voltage one.
- The circuit inputs and outputs must have short circuit and overload protection.
- The chosen electrical components should have an automotive grade, complying with the AEC-Q standards.
- The circuit must be non-programmable and utilize analogue design techniques.

A. Materials

Gigavac GV241BAC was chosen as Accumulator Insulation Relay (AIR), Arcol HS50 10K was used as a pre-charge current limiting resistor, RC4558 was used as a buffering amplifier, LM393 was chosen as a comparator, VOM617A-3T was used as an opto-isolator, SQM100P10-19L was chosen as a P-channel MOSFET. Furthermore, resistors RN73R2BT1D1004B25 and RT1206BRD0760K4L

from KOA Speer and Yageo, respectively, were used to create the voltage divider to step down the high voltage. Resistors TNPW12064K70BEEA, ERA-8AEB154V, and RN73H2BTTD2203F100 from Vishay, Panasonic, and KOA Speer, respectively, were used to create the voltage divider to implement hysteresis and establish threshold levels for the comparator output. Components were powered by the SCWN03A-12 DC-DC converter from MEAN WELL. Additionally, 1714971 Phoenix Contact terminal blocks, 0314.750MXP and 0ADAC0200-BE cartridge fuses, P6KE600A-B, SD12-7 and TPSMB48A-VR transient-voltage-suppression diodes, were used for circuit protection. All of the electrical components were received from Mouser Electronics, Mansfield, Texas, USA. The final prototype PCB was purchased from JLCPCB, Hong Kong, China. Further details on component connections and placement can be seen in the circuit schematic and PCB layout given in Appendixes.

B. Current limiting

A high power resistor in combination with an industrial DC contractor was already chosen by HARD to implement the current limiting functionality. These components essentially created the necessary pre-charge behaviour, as the resistor could limit the flow of inrush current and dissipate the extra energy in the form of heat, while the contractor, connected to the positive accumulator terminal, could bypass the current, omitting the current limiting resistor, during normal operation. Nonetheless, establishing control over pre-charge was the main research objective of this project.

C. Voltage measurement

An operational amplifier IC in combination with a resistive divider was chosen to implement the voltage measuring functionality. Measuring the voltage of the accumulator and the inverter required stepping down the high voltage levels to lower ones through a resistive divider. The formula to calculate the output voltage of a resistive divider is as follows:

$$V_{out} = \frac{V_{in} \cdot R_2}{R_1 + R_2} \quad (2.1)$$

where V_{in} represents the voltage level of the accumulator or the inverter and R_1 and R_2 are the equivalent resistance values of the resistors used to create the divider, shown in Figure 2. A combination of R_1 of $5M\Omega$ and R_2 of $60.4k\Omega$ yielded 7.161V when the accumulator was fully charged to 600V. Stepping down the 600V to less than 10V was appropriated since the desired working voltage of the op-amp was 12V, which was to be powered from the low voltage system in the car (based on a separate isolated $LiFePO_4$ battery). Furthermore, the resistors needed to have a power rating which was high enough to sustain continuous measurement of the voltage of the accumulator and the inverter at the highest possible voltage and ambient temperature - 600V at 60°C (The safety system of the car performed automatic shutdown if the temperature exceeded 60°C). The dissipated power by the resistors (P_R) is a function of the voltage and the current that is being drawn:

$$P_R = V \cdot I \quad (2.2)$$

By picking a resistor value in the megohm range, the current flow could be limited to milliamp range:

$$I_{max} = \frac{V_{max}}{R} = \frac{600V}{5M\Omega + 60.4k\Omega} \approx 0.12mA \quad (2.3)$$

With maximum current flow of 0.12mA, the maximum power dissipation calculated from equation (2.2) is:

$$P_{max} = V_{max} \cdot I_{max} = 600V \cdot 0.12mA = 72mW \quad (2.4)$$

Having such power dissipation, allowed using standard 1206 SMD resistors with $\frac{1}{4}$ Watt power rating. Additionally, the resistance of R_1 was created as the sum of multiple lower value resistors connected in series ($5 \times 1M\Omega$). This design technique spread the total power dissipation across multiple resistors, i.e. it reduced the loading effect on each individual one and added fault tolerance to the circuit with the ability of graceful degradation in case of resistor failure. The tolerance of the resistors was chosen to be 0.1% in order to achieve an accurate step down ratio with minimum possible error. The error of the output of the voltage divider can be obtained based on the worst case scenario calculation using the tolerance values of resistors R_1 and R_2 . The maximum possible output is achieved when 0.1% is subtracted from the nominal value of R_1 and 0.1% is added to the nominal value of R_2 resulting in resistance values $4.995M\Omega$ and 60460.4Ω respectively. Based on equation 2.1, the output voltage is 7.176V when the input voltage is equal to 600V. On the other hand, the minimum possible output voltage is achieved when 0.1% is added to the nominal value of R_1 and 0.1% is subtracted from the nominal value of R_2 , $5.005M\Omega$ and 60339.6Ω respectively. These values calculated for resistors R_1 and R_2 yield an output of 7.147V. Therefore, the output of the voltage divider has a tolerance of $\pm 14.5mV$.

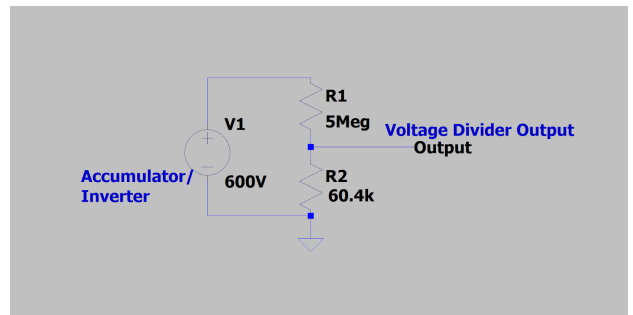


Fig. 2. Generalized voltage divider schematic.

The op-amp's high input impedance was required to prevent subsequent parts of the control circuit from interfering with the voltage level across the voltage divider. The op-amp was used in a voltage buffer configuration to relay the signal from the voltage divider to the comparison stage, shown in Figure 3. This design choice was inspired from an article, published by Texas Instruments, which suggests a method for measuring inverter voltage in EVs [8]. Furthermore, the op-amps, used in the pre-charge control circuit, were selected to have working voltage of 12V, as the low voltage system of

the *HRD05-2* could provide approximately between 10V and 15V DC. A ceramic bypass capacitor of $0.1\mu F$ was connected across the supply lines of the op-amp IC, according to the recommendations of its datasheet - [9], in order to suppress electromagnetic interference (EMI).

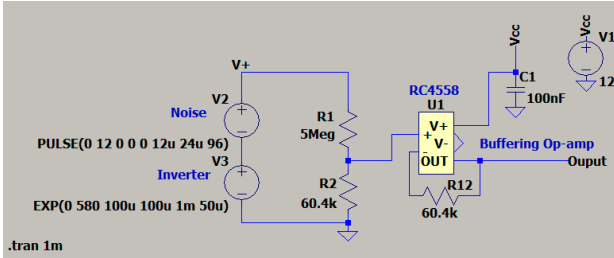


Fig. 3. General Purpose Op-Amp - RC4558, voltage buffer schematic.

D. Voltage comparison

A Comparator IC was chosen to implement the voltage comparison functionality in the pre-charge control circuit. Comparators are optimised for continuous saturated operations and have fast switching speeds which allows the circuit to have a quick response. One of the customer requirements specified that pre-charging should stop once the inverter voltage has reached 95% of the accumulator voltage. That is why the comparator was placed after the buffering op-amps in order to compare the voltage levels of the accumulator and the inverter. The output signal of the accumulator-side buffering op-amp was fed into the non-inverting input of the comparator, while the output of the inverter-side buffering op-amp was fed into the inverting input of the comparator. In this configuration, the output of the Comparator IC is triggered when the inverter voltage becomes larger than the accumulator voltage. In reality, the inverter voltage does not exceed the accumulator voltage. Therefore, the signal on the non-inverting input of the comparator had to be stepped-down, so that the signal on the inverting input could become larger than it. That was also the reason for having the “95%” requirement. To achieve this, once again, a voltage divider was used. A configuration of $4.7k\Omega$ and $150k\Omega$ resistors was placed right before the non-inverting input of the comparator which stepped down the preceding signal to 97% of its value. A ceramic bypass capacitor of $0.1\mu F$ was also connected across the supply lines of the Comparator IC. The resulting circuit is illustrated in Figure 4. Furthermore, implementation of hysteresis was desired to filter out any potential noise affecting the comparator inputs. That is why the Comparator was configured with positive feedback which created an upper and a lower threshold for triggering the Comparator output. A $220k\Omega$ resistor was placed in the feedback path according to a design guideline - [10], that was used to calculate the appropriate resistor value. In this case, pre-charging would be stopped once the inverter voltage reached 98% of the accumulator voltage and re-initiated if it fell below 95%.

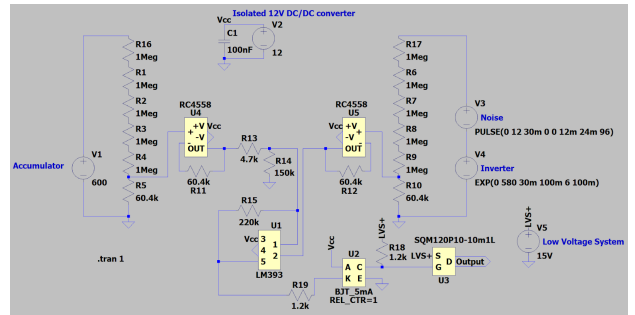


Fig. 4. Comparator IC - LM393, voltage comparison schematic.

E. Power supply

Both ICs - Comparator and op-amp, had to be powered from the low voltage system through a 12V regulated power supply, which has an isolation rating of at least three times the maximum accumulator voltage. Such power supply was necessary to maintain galvanic isolation between the high voltage and low voltage systems, and because the low voltage system could provide at maximum 15V DC when fully charged. The 12V isolated DC/DC converter - SCWN03A-12 from MEAN WELL, was chosen to be used, as it has an input range of 9 to 18V, 3kV isolation rating, and maximum output power of 3W. The negative output terminal of the DC/DC converter had to be electrically connected to the negative terminal of the accumulator in order to create a shared reference between the tractive system and the voltage measuring/comparing devices.

F. Controlling AIR

After having implemented the necessary voltage measurement and comparison functionality, the next step involved utilizing the output signal of the Comparator to control the state of the AIR connected to the positive terminal of the accumulator. To achieve this, a combination of an optocoupler and a P-channel MOSFET was used. All the components, necessary for the voltage measurement and comparison functionality, were directly connected to, either, the accumulator or the inverter of the car (i.e. high voltage system/HVS), while the MOSFET, used to energize/de-energize the coil of the AIR, was connected to the low voltage system (LVS). The optocoupler was necessary to maintain galvanic isolation between the high voltage and low voltage systems, i.e. it was used to create electrical separation between the Comparator and the MOSFET. The anode pin of the optocoupler was connected to the positive supply line of the DC/DC converter, while the cathode pin was connected to the output pin of the Comparator, because the output stage of the chosen Comparator - LM393, is of open-collector type (i.e. triggered output entailed that the output pin sank current). A resistor of $1.2k\Omega$ was placed between the cathode pin and the output pin of the Comparator in order to limit the current flow, as the chosen optocoupler - VOM617A-3T, has a minimum required input current of 5mA and a maximum of 60mA. Additionally, an LED was placed on the output stage of the optocoupler to indicate the

result of the comparison. A P-channel MOSFET was needed because the output stage of the optocoupler is, also, of open-collector type and the coil of the AIR had to be energized once the output of the optocoupler was triggered. Therefore, the gate pin of the MOSFET was connected to the positive supply line of the DC/DC converter through a $1.2k\Omega$ resistor, as the output of the optocoupler has a maximum current rating of 50mA. Furthermore, the chosen MOSFET needed to have drain-source breakdown voltage higher than the maximum possible back EMF from the AIR coil - 55 V, and it had to be able to sustain the pick up current of the AIR - 3.9A. It also needed to have a power rating which was high enough at 60°C to dissipate the continuous coil current of 230mA across the on-resistance. The P-channel MOSFET - SQM100P10-19L from Vishay, with AEC-Q101 qualification, was chosen to be used, as it features $19m\Omega$ on-resistance and -100V drain-source breakdown voltage. The resulting circuit is illustrated in Figure 5. One of the last considerations that were made,

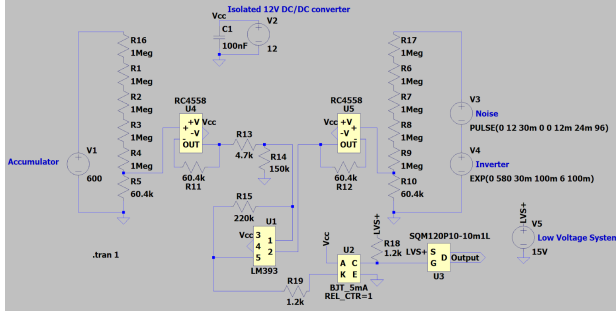


Fig. 5. Pre-charge control schematic.

included implementation of circuit protection, as the circuit was designed predominantly with surface-mount components, which are known to be vulnerable to electrostatic discharge (ESD). To protect the circuitry against potential ESD strikes, transient-voltage-suppression (TVS) diodes were added to the inputs and outputs of the final circuit. The TVS diodes at the accumulator and inverter connectors needed to suppress voltage transients which exceeded 600V, while the TVS diode at the input of the DC/DC converter needed to suppress transients exceeding 18V. The TVS diode at the output stage of the MOSFET was selected to have a clamping voltage of more than 55V because it needed to suppress transients without suppressing the back-EMF of the AIR. Furthermore, fast-blow cartridge fuses were added at the inputs to protect in case of short circuits. The accumulator and inverter connectors were fused for 200mA, while the input of the DC/DC converter was fused for 750mA, as recommended by the datasheet of the device [11]. The final circuit is illustrated in Figure 6.

G. PCB layout

A main safety concern in the design of the physical board included establishing clearance between the low and the high voltage sides of the board. In order to maintain isolation, a clearance of at least 12.7 mm was required between the two sides. Furthermore, the width of copper traces was calculated

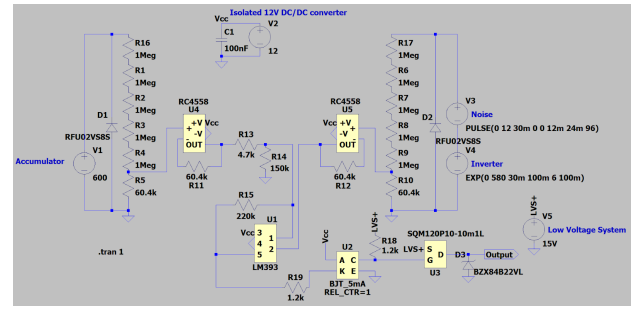


Fig. 6. Final pre-charge control circuit schematic.

according to the current flow in each section. Most importantly, the LVS side had to sustain current flow of 10 A in order to guarantee operation of the AIR. This resulted in choosing copper traces with 4 mm width and 2 oz/ft² thickness [12].

III. RESULTS

The performance of the circuit was, at first, studied using a circuit simulation software - LTspice. The final schematic was imported into the simulation environment and different points of the circuit were analyzed. Figure 7 depicts the charging behavior of the inverter which acts as one of the inputs to the circuit. The input signal was exponentially increased from 0V to 600V, resembling the charging behaviour of a capacitor. Additionally, 200mV peak-peak noise was added to the signal in the form of a sinusoid.

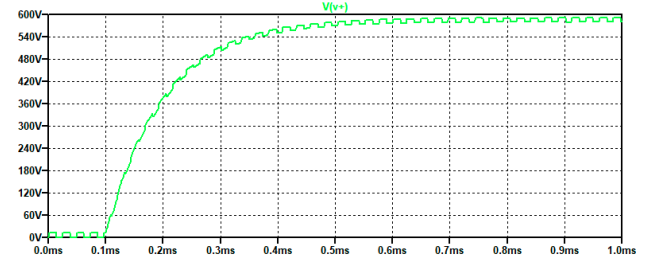


Fig. 7. Input signal of the voltage divider.

The output signal of the voltage divider was then fed into the unity-gain amplifier whose output is illustrated in Figure 8.

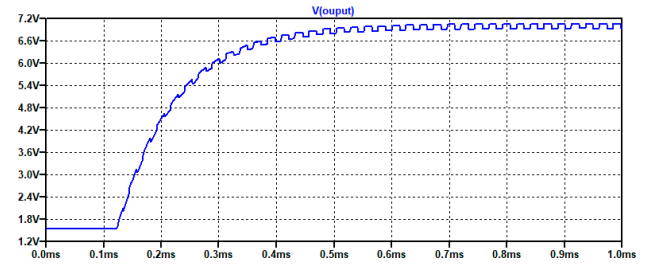


Fig. 8. Output signal of the buffering op-amp.

The buffered voltages from the accumulator and inverter were then fed into the non-inverting and inverting input of the comparator. The system response is shown in Figure 9

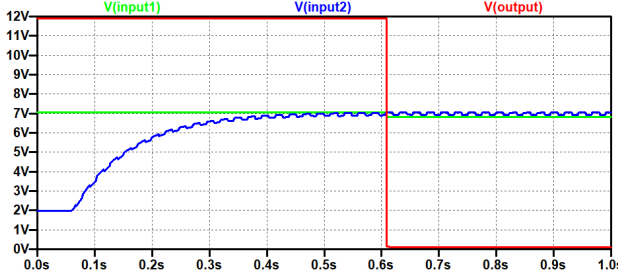


Fig. 9. Comparator output based on the input signals. Input 1 illustrates the accumulator voltage while input 2 depicts the charging of the inverter capacitors.

The output of the comparator starts sinking current once the inverter voltage reaches 98% of the accumulator voltage - 7.04V, based on the hysteresis calculation. This causes the output signal to switch from 12V to 0V. Moreover, the output of the optocoupler also switches from HIGH to LOW state which is then used as the control signal for the MOSFET, seen in Figure 10. A LOW state causes the MOSFET to close the circuit and 12V to appear at the output of the circuit enabling it to close the accumulator insulation relay, ending the pre-charge process.

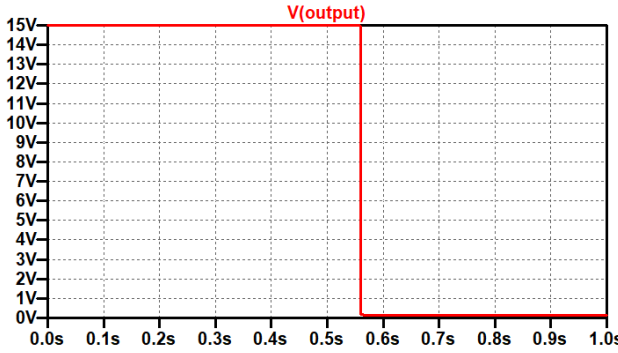


Fig. 10. Output signal of the optocoupler.

Finally, ESD immunity test was conducted in software, utilizing a ESD generator model whose output characteristics have been designed in accordance with the IEC 61000-4-2 standard, illustrated in Figure 11. An 8kV direct contact discharge was simulated at locations that were most vulnerable to an ESD strike and, therefore, were protected with TVS diodes. Input of the voltage divider, output of the circuit, and input of the low voltage system were probed and the results suggest that the diodes limit the voltage to their specified clamping voltage, hence, providing overvoltage protection. Furthermore, the pre-charge control circuit performance was evaluated with low-voltage tests in real life. The collected data is shown in Table I. Hysteresis percentage of comparator output was measured using a lab power supply, multimeter and a climate chamber. Three different people carried out the measurements with one prototype board. A Gage R&R analysis of the collected data indicated that components characteristics had the biggest influence on the total variation

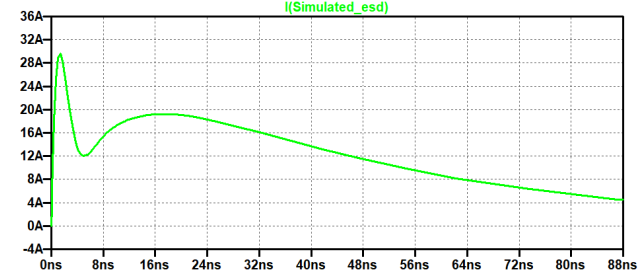


Fig. 11. The current waveform of a simulated ESD strike as defined by IEC 61000-4-2.

in the measurements and 80% of the measurement error can be attributed to them.

Operator	Trial #	Setpoint					
		10 °C	20 °C	40 °C	50°C	60 °C	65 °C
Operator Pedro	1	97.07	97.07	96.93	95.81	93.58	93.02
	2	96.93	97.21	96.93	95.81	93.58	93.02
	3	96.93	97.21	96.93	95.95	93.58	93.02
	\bar{X}	96.98	97.16	96.93	95.86	93.58	93.02
	R	0.14	0.14	0.00	0.14	0.00	0.00
Operator Richard	1	97.07	97.07	96.79	95.81	93.58	93.02
	2	97.07	96.93	96.65	95.67	93.58	93.02
	3	96.93	97.07	96.65	95.81	93.58	93.02
	\bar{X}	97.02	97.02	96.70	95.76	93.58	93.02
	R	0.14	0.14	0.14	0.14	0.00	0.00
Operator Dimitriy	1	97.07	97.07	96.79	95.81	93.58	93.02
	2	97.07	96.93	96.65	95.67	93.58	93.02
	3	96.93	97.07	96.65	95.81	93.58	93.02
	\bar{X}	97.02	97.02	96.70	95.76	93.58	93.02
	R	0.14	0.14	0.14	0.14	0.00	0.00
\bar{X}		97.01	97.07	96.77	95.79	93.58	93.02
R		0.14	0.14	0.09	0.14	0.00	0.00

TABLE I
EXPERIMENTAL VARIATION DATA COLLECTED FROM CLIMATE CHAMBER TESTS. UPPER THRESHOLD OF HYSTERESIS (%).
 \bar{X} – Average, R – Range

The data suggests that the comparator output experiences temperature dependence. This is further illustrated in Figure 12. Above 50 °C the observed parameter fails to meet specifications. This prompted an extended troubleshoot, during which a design flaw was discovered. When examining the Comparator inputs at higher temperatures, illustrated in Figure 13, a strong electromagnetic interference of 560mV peak-peak was uncovered. The magnitude of the interference was high enough to disturb the output of the Comparator.

The origin of the induced noise was traced back to the operational amplifier which appeared to amplify the input signal. Starting with 160mV at the input and ending with 360mV at the output, Figure 14, inferred that the op-amp had an amplification factor of 2.25.

Nevertheless, the circuit did not fail to meet specifications in the temperature range +10 °C to +40 °C. Figure 15 (top)

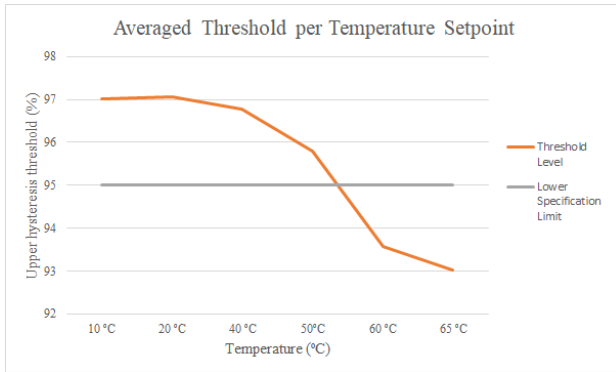


Fig. 12. Measurement of upper threshold of hysteresis at different temperatures.

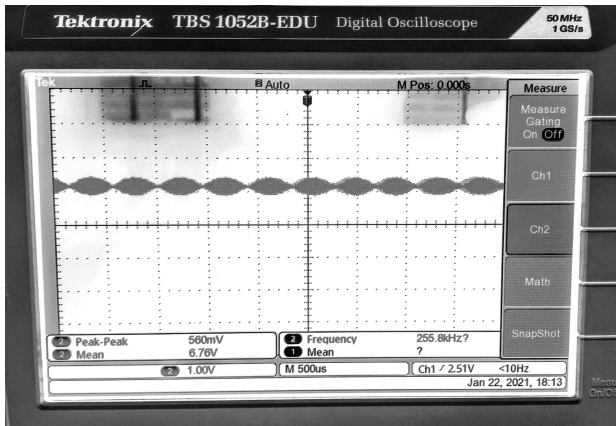


Fig. 13. Oscilloscope measurement of the Comparator's input signal at 65 °C. 560mV p-p EMI.

depicts the LOW output state of the circuit when the voltage level of channel 2 was less than 95% of the voltage level of channel 1 of the power supply. Figure 15 (bottom) shows the triggered HIGH state of the output when channel 2 exceeded 98% of channel 1.

IV. DISCUSSION

Additional experiments can be conducted to further confirm the suitability of the designed circuit. A high voltage power supply can be used to test the circuit's ability to sustain and 600V. Operation of the AIR can result in peak current draw of 10A. The copper traces of the PCB and the components that are part of the high current path should be inspected to verify their capability of withstanding currents up to 10A. Moreover, it is important to determine the total resistance of the electrical path on the LVS side of the circuit. High current consumption along with high resistance can cause considerable voltage drop across the components which can decrease the ability of the LVS to close the AIR. The behaviour of the designed circuit proved inconsistent compared to the simulation in LTspice. The presence of a 60.4k resistor in the feedback path of the buffering amplifier yielded an amplification factor of 2, instead of 1 as simulation suggested. The consequences of having an

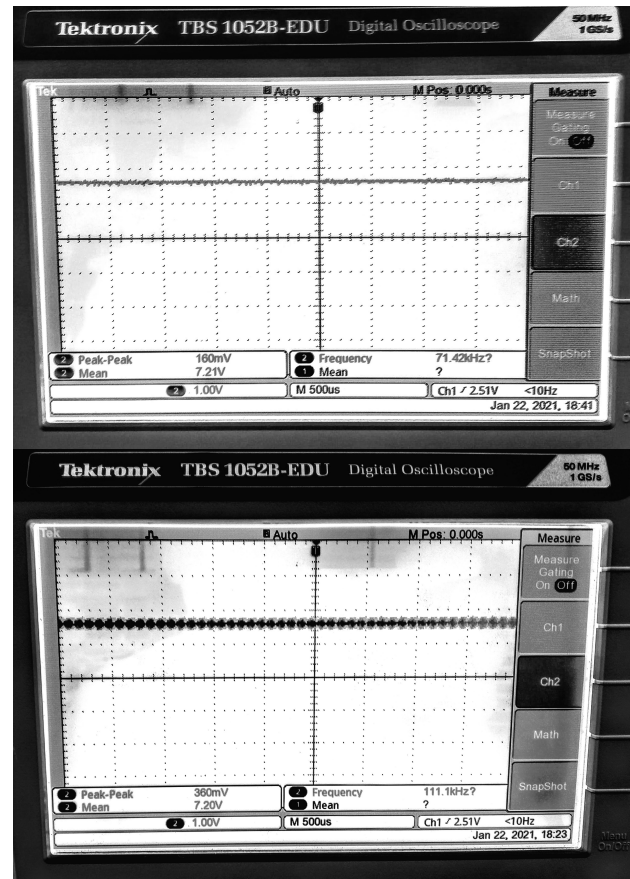


Fig. 14. Oscilloscope measurement of the op-amp's input and output signal. Input (top) 160mV p-p EMI. Output (bottom) 360mV p-p.

operational amplifier with gain of 2 were significant as the magnitude of the induced EMI was high enough to disturb the hysteresis of the Comparator. Using a filtering technique, such as a low pass filter at the input terminals of the op-amp may prove beneficial for the stability of the circuit. The climate chamber test results, also, suggest that the circuit experienced temperature dependence. This can be explained by the further increase in amplification of the op-amp due to temperature change. It is also reasonable to question whether the chosen package size of the Comparator IC was appropriate. The LM393PWR (Comparator IC) has a TSSOP-8 package, which is one of the smallest available. Bigger component packages may contribute for a better heat dissipation and decrease temperature dependence. Nevertheless, the problem was resolved by removing the resistors in the feedback path of the op-amp and replacing them with shorts, illustrated in Figure 16. The decision of having feedback resistors at the first place was based on a design guideline which suggested that having equal resistance at both inputs of the op-amp will result in equating the input bias currents, hence reducing error due to bias current mismatch. However, the bias current in particular for the RC45558 is of nano-amp magnitude. Combining this with an amplification factor of 1 would certainly not affect the measurements. The amplification problem seems to have

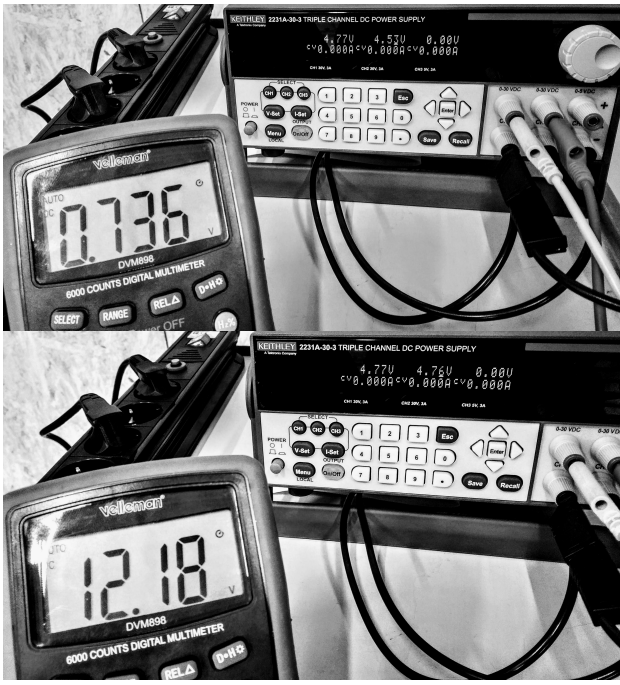


Fig. 15. Multimeter measurement of the AIR's control signal. Output state - LOW & Output state - HIGH.

arisen due to inaccurate configuration of the resistors that establish a non-inverting unity-gain amplifier.

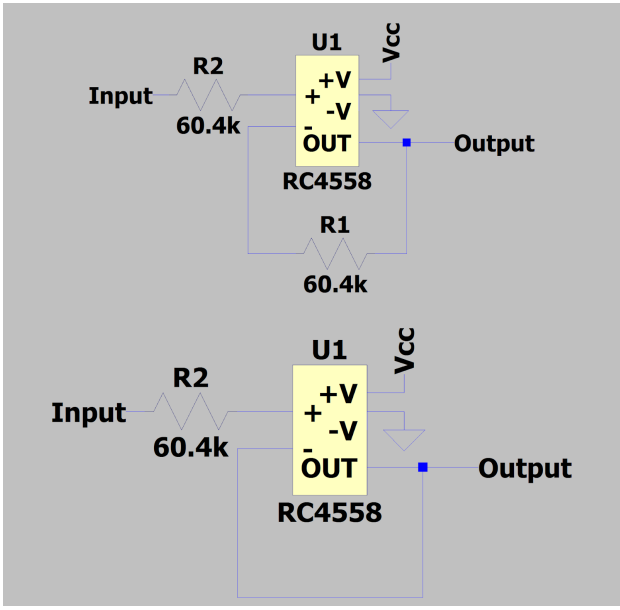


Fig. 16. Buffering op-amps fix - removing feedback resistor. Comparison between old design (top) and new one (bottom).

After resolving the op-amp issue, the circuit seemed to perform as expected in the tested temperature range - +10 °C to +65 °C. More specifically, pre-charge state occurred if the inverter voltage was below 95.11% of the accumulator voltage, while normal operation continued once it exceeded 98.32%.

Finally, in case budget is of less concern, replacing the commercial off-the-shelf (COTS) components with industrial-grade (AEC, AQEC, or QML) ones will guarantee reliability and prolonged operation of the circuit in the environment of the racing car. In the pursuit to improve quality, both the RC4558 and LM393 can be replaced with the LM2904B-Q1 and LM2903B-Q1, respectively.

V. CONCLUSIONS

Establishing a reliable connection between the accumulator and the inverter of an EV is essential. The presented pre-charge control circuit is a potential solution that can be used to operate an accumulator insulation relay and prevent the flow of high inrush current. The circuit is characterised with an analogue design, galvanic isolation, and hysteresis in comparison of the voltage levels. Pre-charging is stopped once the inverter voltage exceeds 98% of the voltage level of the accumulator and resumed when it is below 95%. The simulation environment LTspice was a valuable tool during the design stage of the circuit and proved to be effective for testing. Nonetheless, the results of simulation are dependent on the quality of the models of the components and do not fully represent reality. Further testing is required to verify the operation of the circuit across a wide voltage range.

ACKNOWLEDGMENT

We thank Prof. Pedro Gomes Lourenço for his dedication in giving the Research Skills course at Hanze Institute of Technology, Assen.

APPENDIX A. CIRCUIT SCHEMATIC

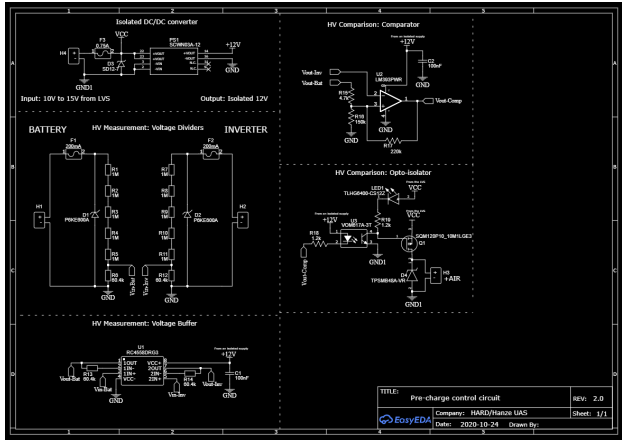


Fig. 17. Circuit schematic, EasyEDA.

APPENDIX B. PCB LAYOUT

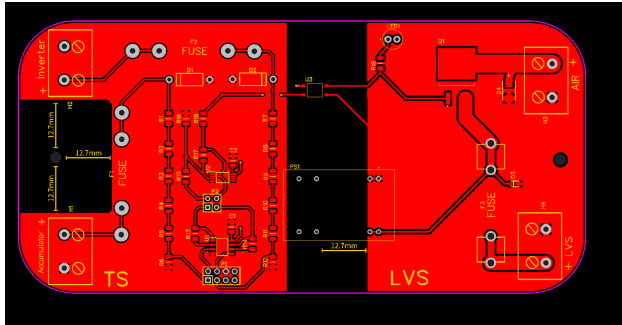


Fig. 18. PCB layout, EasyEDA.

REFERENCES

- [1] IEA (2020), "Global EV Outlook 2020", IEA, Paris.
- [2] "Rules for FSG 2020", Formulastudent.de, 2020.
- [3] V. van der Woude, Team Manager, Hanze Racing Division, personal communication, Sept. 2020.
- [4] C. Siskind, Electrical Control Systems in Industry. New York: McGraw-Hill, 1963.
- [5] N. Sugliano, "Proficiency testing for calibration of multimeter," in 19th International Congress of Metrology, 2019.
- [6] T. Kuphaldt, "Divider circuits and Kirchhoff's law" in Lessons in Electric Circuits, vol. 1, 2000.
- [7] G. Brue and R. Launsby, Design for Six Sigma. New York: McGraw-Hill, 2003.
- [8] "High-Accuracy Isolated Voltage Measurements in HEV/EV", Ti.com, 2020.
- [9] "RC4558 Dual General-Purpose Operational Amplifier", Ti.com, 2014.
- [10] "Comparator with Hysteresis Reference Design", Ti.com, 2020.
- [11] "3W DIP Package DC-DC Regulated Converter SCWN03 & DCWN03 Series", meanwellusa.com, 2020.
- [12] "Printed Circuit Board Trace Width Tool, Advanced Circuits", 4pcb.com.